Suitability of the Kihara Potential To Predict Molecular Spectra of Linear Polyatomic Liquids

S. Calero,[†,‡] B. Garzón,[§] S. Jorge,[‡] J.A. Mejías,[†] J. Tortajada,[‡] and S. Lago*[,†]

Facultad de Ciencias Experimentales, Carretera de Utrera, Km 1, Universidad Pablo de Olavide, 41013 Seville, Spain; Departamento Química Física, Facultad de Ciencias Químicas, Universidad Complutense, 28040 Madrid, Spain; and Departamento Ciencias Básicas, Facultad de Ciencias Experimentales y Técnicas, Universidad San Pablo CEU, Urbanización Montepríncipe, Boadilla del Monte, 28660 Madrid, Spain

Received: November 4, 1999; In Final Form: February 4, 2000

Gibbs ensemble Monte Carlo (GEMC) simulations of linear molecular liquid chlorine and carbon disulfide are performed to determine the vapor−liquid equilibrium (VLE) of these fluids and the corresponding intermolecular potential parameters. The intermolecular potential function considered is the Kihara potential with a point multipole added. Molecular dynamics runs of liquid nitrous oxide, chlorine, and carbon disulfide are then presented to obtain angular velocity autocorrelation functions of different orders. Using these functions, transport coefficients as well as correlation times are calculated. Next, the band shapes of molecular vibration spectra are obtained as Fourier transforms of the autocorrelation functions. Agreement between experiment and simulation is excellent for all the calculated properties of chlorine, showing that the intermolecular potential presented here is extremely accurate as well as simple. Results for carbon disulfide and nitrous oxide range from very good to acceptable for different correlation times and transport properties and they are discussed in detail in the text.

I. Introduction

Intermolecular forces and statistical mechanics are two general key terms used in relation to liquid state physical properties. Thermodynamic and dynamic properties of liquids composed of monatomic molecules are well described by simple intermolecular potentials,[1] such as Lennard-Jones, square-well, or Stockmayer potentials. The situation is not so clear in the case of polyatomic liquids, where intermolecular forces depend on the mutual orientations of molecules. In this case, the most popular intermolecular potential is the *n*-center Lennard-Jones potential, written as a sum of individual Lennard-Jones-like contributions for each pair of atoms or molecular sites.[2] This potential is particularly useful when interpreting X-ray or neutron diffraction[3,4] data, but its complexity rapidly grows with the number of chemically different atoms included in the molecule. So, for such a simple molecule as ethanol, the number of different site−site interactions can be as high as 21. In this and in more complicated cases, the potential becomes unmanageable and drastic simplifications, either by reducing the number of sites or by other means, are necessary.

To model some substances, alternative ways may sometimes include different potential functions such as the Gay−Berne potential[5,6] or the Kihara potential.[7] The latter has been widely used by several groups[8−13] to obtain thermodynamic properties, notably the vapor−liquid equilibrium of models[14] and actual systems of linear or pseudolinear molecular liquids.[15] Moreover, a variety of theories[16−21] and simulation[22−24] techniques have been used. The Kihara potential is also very popular in several fields related to chemical engineering to calculate properties of gas hydrates[25−29] as well as transport properties and some simple dynamic properties,[30−31] and it has been used recently in different theoretical frameworks.[32−34] Indeed, a similar potential has been suggested for helical molecules such as proteins.[35] In spite of its wide use, we are aware of only one paper using this potential for spectroscopic applications specifically concerning the problem of stability of solid phases of linear molecules.[36]

The main aim of this paper is to evaluate how well this particular potential works to predict some typical spectroscopic liquid state properties, as in the Raman spectrum of linear nonpolar molecules such as Cl_2, or in the infrared spectrum of molecules such as N_2O or S_2C. In all these cases, we consider that intermolecular and intramolecular vibrations are well separated and we restrict the study to the highest frequency intramolecular vibration in polyatomic molecules. The intermolecular interaction in the liquid causes a band broadening and frequency shift with respect to the ideal gas phase spectrum. The band broadening is related to the Fourier transform of the different order Legendre polynomials of molecular angular velocity (AVCF), and the line width is related to the correlation time[37] characterizing the decay of the AVCF. This information is readily obtained from our molecular dynamics simulations. The frequency shift due to the condensed phase effect is estimated in a simple way, considering the perturbation due to the intermolecular potential on the total molecular potential. Parameters for N_2O are taken from a previous paper,[38] and we have performed additional Gibbs ensemble Monte Carlo (GEMC) simulations for S_2C and Cl_2 to obtain the VLE using a Kihara plus a multipole−multipole interaction, as described in section II.

Once the intermolecular potential parameters were obtained, we carried out molecular dynamics simulations at the temper-

* To whom correspondence should be addressed. Phone: 00-3495-4349309. Fax: 00-3495-4349238. E-mail: slagara@dex.upo.es.
[†] Universidad Pablo de Olavide.
[‡] Universidad Complutense.
[§] Universidad San Pablo CEU.

10.1021/jp993904j CCC: $19.00
Published on Web 05/27/2000

atures and densities where spectroscopic data exist. Results for the different correlation functions and for transport coefficients for the molecules considered here are also shown in section III. Our results in section IV show that we can calculate the shape of the chlorine spectrum very accurately, using the same parameters estimated from VLE. Results for the other molecules are also very satisfactory in general. Finally, section V presents some conclusions and general remarks.

II. Fitting of Potential Parameters

We have performed Monte Carlo simulations in the Gibbs ensemble (GEMC) to fit the molecular potential parameters to the experimental vapor−liquid equilibrium (VLE). Molecules interact through the Kihara potential plus a multipole interaction. Details of simulations and pertinent equations are given elsewhere.[14,24,39] The molecular core is taken as a linear segment in all the cases considered here and the model length and multipole moment are chosen to reproduce the experimental critical values exactly and to approximate the experimental multipoles[40−42] of real molecules. Indeed, experimental values for multipoles are considerably scattered and we have performed independent quantum mechanical calculations using density functional theory (DFT), as explained below, to obtain confident values. Experimental and fitted values are shown in Table 1 for the molecules considered in this work. Explicitly, the intermolecular potential is written as

$$u = u^{K} + u^{\mu\mu} + u^{QQ} + u^{\mu Q} \quad (1)$$

where the different potential terms are given by

$$u^{K} = 4\epsilon[(\sigma/\rho)^{12} - (\sigma/\rho)^{6}] \quad (2)$$

$$u^{\mu\mu} = \frac{\boldsymbol{\mu}_1\cdot\boldsymbol{\mu}_2}{r^3} - \frac{3(\boldsymbol{\mu}_2\cdot\mathbf{r})(\boldsymbol{\mu}_2\cdot\mathbf{r})}{r^5} = \frac{\mu^2}{r^3}(c\nu_{12} - 3c_1c_2) \quad (3)$$

$$u^{QQ} = \frac{3Q^2}{4r^5}(1 - 5c_1^2 - 5c_2^2 - 15c_1^2c_2^2) + \frac{3Q^2}{4r^5}(2(c\nu_{12} - 5c_2c_2)^2) \quad (4)$$

$$u^{\mu Q} = \frac{3\mu Q}{2r^4}c_{12}(1 + 5c_2c_2 - 2c\nu_{12}) \quad (5)$$

for the dispersion, dipole−dipole, quadrupole−quadrupole, and dipole−quadrupole interactions, respectively. In the eq 2, ρ is the shortest distance between molecular cores, and ϵ and σ are the potential parameters with dimensions of energy and length, respectively. Moreover, $c_i = \cos\theta_i$, $s_i = \sin\theta_i$, $c_{12} = \cos(\theta_1 - \theta_2)$ and $c\nu_{12} = \cos\nu_{12} = \mathbf{e}_1\cdot\mathbf{e}_2 = \cos\theta_1\cos\theta_2 + \sin\theta_1\sin\theta_2\cos(\phi_1 - \phi_2)$ in the eqs 3, 4, and 5. Angles are defined as in Figure 1 of ref 24. Intermolecular interaction parameters were obtained by fitting the model critical values to the experimental critical values of each substance[43−45] and are also shown in Table 1. Details of the fitting are given elsewhere[15] and VLE for nitrous oxide has been recently published.[38] Figure 1 shows the VLE curve and vapor pressure of chlorine versus the temperature. Simulations were only performed at the thermodynamic states shown in Table 2 but a smooth extrapolation is possible and agreement with experiment[46] is excellent for chlorine over a very broad temperature range. In this case, the inclusion of a point quadrupole significantly improves the very good agreement reported for previous nonpolar models.[15,17,47] Moreover, the inclusion of a quadrupole provides a simple mechanism to explain the vibration frequency shift in the liquid state as shown below. Note that in the case of chlorine, we neglect here the small differences between potential parameters of isotopic species. However, the isotopes have markedly different transport and spectroscopic properties, as shown below.

TABLE 1: Critical Properties, Intermolecular Potential Parameters, and Multipole Moments for the Molecules Considered in This Work

properties[a]	Cl_2	S_2C	N_2O
T_c (K)	416.95[43]	549.4[44]	309.6[45]
ρ_c (mol/L)	8.13[43]	5.8105[44]	10.264[45]
p_c (bar)	75[43]	78.8[44]	72.4[45]
Z_c	0.29	0.293	0.274
ϵ/k (K)	417.42	584.27	318.8[38]
σ (A)	3.208	3.368	2.82[38]
L^*	0.625	0.9	0.8[38]
$L^{(exp)}$ (A)	1.988[46]	3.108[46]	2.317[46]
$L^{(GEMC)}$ (A)	2.005	3.031	2.280
μ^{*2}	0	0	0.7
$\mu^{(exp)}$ (D)	0	0	0.166[40]
$\mu^{(GEMC)}$ (D)	0	0	0.846
$\mu^{(DFT)}$ (D)	0	0	0.12
Q^{*2}	0.295	0.7	0.15
$Q^{(exp)}$ (B)	2.994[41]	3.597[42]	-
$Q^{(GEMC)}$ (B)	2.405	4.948	1.116
$Q^{(DFT)}$ (B)	2.99	2.94	3.49

[a] Debye (D) and Buckingham (B) are the common experimental units and their equivalence in SI units are 3336×10^{-30} C m for Debye and 3336×10^{-40} C m^2 for Buckingham. Values that are not referenced are calculated in this work.

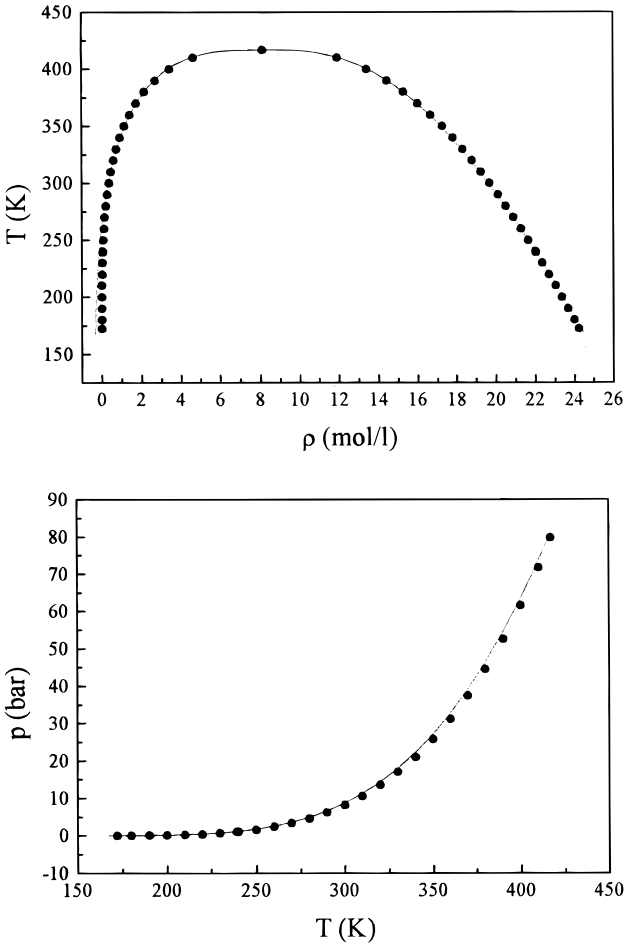

Figure 1. (a) Vapor−liquid equilibrium coexistence densities for the fluid Cl_2. Circles are experimental points. Continuous line is a fitting to our simulation results. (b) Vapor pressure of liquid Cl_2 as a function of temperature. Symbols as above.

TABLE 2: Vapor−Liquid Coexistence Properties of Molecular Liquids Considered in This Work As Obtained from GEMC Simulations Using the Intermolecular Parameters of Table 1

T (K)	ρ_g (mol/l)	ρ_l (mol/l)	P (bar)	ΔH_v (kJ/mol)
		Chlorine		
388.21	2.37 ± 0.13	14.55 ± 0.89	51.1 ± 2.8	7.30 ± 0.73
384.03	2.13 ± 0.11	14.56 ± 0.70	46.6 ± 2.4	7.49 ± 0.60
379.86	2.32 ± 0.12	15.57 ± 0.46	48.0 ± 2.4	8.16 ± 0.44
375.68	2.17 ± 0.15	15.78 ± 0.65	45.8 ± 2.4	8.42 ± 0.60
365.25	1.65 ± 0.11	16.42 ± 0.39	36.6 ± 1.9	9.33 ± 0.42
354.81	1.34 ± 0.17	16.93 ± 0.44	30.2 ± 2.9	9.99 ± 0.56
344.38	1.08 ± 0.13	17.49 ± 0.36	24.6 ± 2.4	10.72 ± 0.50
333.94	0.83 ± 0.06	18.02 ± 0.29	20.3 ± 1.3	11.29 ± 0.36
323.51	0.65 ± 0.07	18.58 ± 0.22	15.2 ± 1.4	12.13 ± 0.39
313.07	0.51 ± 0.07	19.05 ± 0.21	10.6 ± 1.4	12.94 ± 0.45
		Carbon Disulfide		
528.77	2.19 ± 0.16	8.93 ± 1.67	58.56 ± 5.25	7.77 ± 2.29
525.85	2.21 ± 0.06	10.34 ± 0.60	57.14 ± 4.14	9.58 ± 0.95
522.93	1.86 ± 0.08	9.80 ± 0.78	52.16 ± 2.68	9.24 ± 1.18
517.09	1.87 ± 0.07	10.18 ± 0.96	51.32 ± 2.70	9.63 ± 1.46
511.24	1.84 ± 0.11	10.72 ± 0.57	49.14 ± 3.12	10.69 ± 0.93
496.64	1.28 ± 0.07	11.22 ± 0.37	37.50 ± 2.17	12.73 ± 0.67
482.03	1.03 ± 0.06	11.77 ± 0.30	31.15 ± 1.86	13.52 ± 0.59
467.42	0.83 ± 0.07	12.33 ± 0.24	24.98± 1.67	14.82 ± 0.54
452.82	0.67 ± 0.06	12.71 ± 0.23	20.34 ± 1.58	15.82 ± 0.57

Experimental quadrupole moment results are in general widely scattered, strongly depending on the experimental method, and this experimental inaccuracy may shed some doubts on the physical meaning of our fitted parameters. To clarify this point, we have also computed multipole moments from charge distributions obtained from different quantum mechanical methods.[48−51] The calculations are made with two different high-quality basis sets. The first one is the 6-31G†† basis set[48] and the second one, 6-31+G(3df,2p), is a 6-31G basis set supplemented by diffuse functions,[49] three sets of d functions and one set of f functions on heavy atoms, and two sets of p functions on hydrogens.[51]

The most satisfactory agreement between experiment, quantum computations, and simulation parameters for chlorine is obtained when geometry and charge distribution come from density functional theory (DFT) ab initio calculations and when the Becke+Perdew−Wang-91 exchange correlation functionals (B-PW91) are used. Multipole moments obtained from this method are shown in Table 1. Simulation results for VLE of the Kihara model of S_2C were not reported previously. As shown in Figure 2, agreement with experiment[52,53] for S_2C is also very good, especially at temperatures close to those where the spectra were obtained. We have also computed charge distributions and quadrupole moments of S_2C and N_2O using the methods referred to above. In both these cases the most favorable agreement with the experiment is obtained with the same approximations as for chlorine. All these results are also shown in Tables 1 and 2 and the agreement with our fitting parameters is fair.

III. Molecular Dynamics Runs

We have performed molecular dynamics simulations for the three molecules considered here, using the potential parameters obtained in the preceding section. Force exerted by a molecule 2 on molecule 1 is

$$\mathbf{f}_{12} = -\left(\frac{\partial u_{12}}{\partial \mathbf{r}_{12}}\right)_{\omega_1,\omega_2} = \mathbf{f}^{K} + \mathbf{f}^{\mu\mu} + \mathbf{f}^{QQ} + \mathbf{f}^{\mu Q} \qquad (6)$$

and the corresponding intermolecular forces are given by

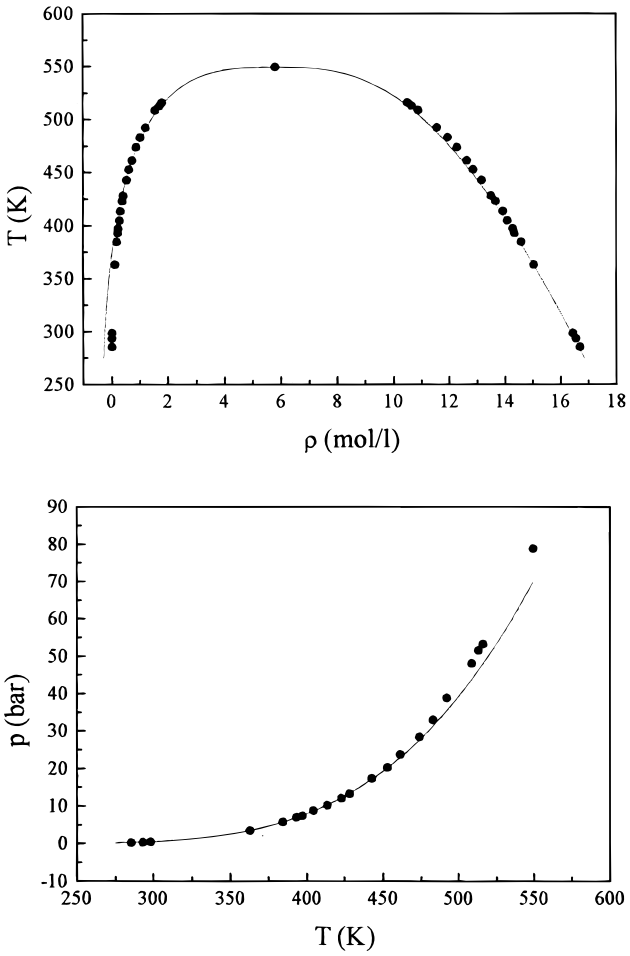

Figure 2. (a, top) Vapor−liquid equilibrium coexistence densities for the fluid S_2C. Circles are experimental points. Continuous line is a fitting to our simulation results. (b, bottom) Vapor pressure of liquid S_2C as a function of temperature. Symbols as above.

$$\mathbf{f}^{K} = -\left(\frac{\partial u_{12}^{K}}{\partial \mathbf{r}_{12}}\right)_{\omega_i,\omega_j} = -\frac{\partial u_{12}^{K}}{\partial \rho_{12}}\cdot\boldsymbol{\mu}_{12} = \left(\frac{24}{\rho_{12}^{8}} - \frac{48}{\rho_{12}^{14}}\right)\cdot\boldsymbol{\mu}_{12} \qquad (7)$$

corresponding to the Kihara interaction, where $\boldsymbol{\mu}_{12}$ is the unit vector in the direction of the shortest distance between molecular cores

$$\mathbf{f}^{\mu\mu} = -\left(\frac{\partial u_{12}^{\mu\mu}}{\partial \mathbf{r}}\right)_{\omega_1,\omega_2} = \frac{3\mu^3}{r^4}\left[(5c_1c_2 - c\nu_{12})\frac{\mathbf{r}}{r} - c_1\mathbf{e}_2 - c_2\mathbf{e}_1\right] \qquad (8)$$

corresponding to the dipole−dipole interaction: $\mathbf{e}_1$ and $\mathbf{e}_2$ are unit vectors in the directions of the molecular axes

$$\mathbf{f}^{QQ} = -\left(\frac{\partial u_{12}^{QQ}}{\partial \mathbf{r}}\right)_{\omega_1,\omega_2}$$

$$= \left\{\frac{5u^{QQ}}{r^2} + \frac{3Q^2}{2r^7}\cdot(10c_1^2 + 10c_2^2 + 60c_1^2\cdot c_2^2 + 80(c\nu_{12} - 5c_1^2\cdot c_2^2)\cdot c_1^2\cdot c_2^2)\right\}\cdot\mathbf{r} - \frac{3Q^2}{4r^6}\cdot(10c_1^2 + 30c_1\cdot c_2^2 + 40\cdot(c\nu_{12} - 5c_1^2\cdot c_2^2)\cdot c_1^2\cdot c_2^2)\cdot\mathbf{e}_1 - \frac{3Q^2}{4r^6}\cdot(10c_2^2 + 30c_2\cdot c_1^2 + 40\cdot(c\nu_{12} - 5c_1^2\cdot c_2^2)\cdot c_1^2\cdot c_2^2)\cdot\mathbf{e}_2 \qquad (9)$$

corresponding to the quadrupole−quadrupole interaction and

$$\mathbf{f}^{\mu Q} = -\frac{4}{r^2}u^{\mu Q}\cdot\mathbf{r} + \left(\frac{\mathbf{e}_1}{r} - \frac{c_1}{r^2}\mathbf{r}\right)\left(\frac{3\mu Q}{2r^4}(-(1+5c_1c_2) - c\nu_{12}) + c_{21}\cdot 5c_2\right) + \left(\frac{\mathbf{e}_1}{r} - \frac{c_{21}}{r^2}\mathbf{r}\right)\left(\frac{3\mu Q}{2r^4}((1+5c_1c_2) - c\nu_{12}) + c_{21}\cdot 5c_2\right) \quad (10)$$

corresponding to the dipole−quadrupole interaction.

To implement our molecular dynamics algorithm, we also need the turning forces that one molecule exerts on another. These turning forces are respectively

$$\mathbf{g}_{12} = \mathbf{g}^{K} + \mathbf{g}^{\mu\mu} + \mathbf{g}^{QQ} + \mathbf{g}^{\mu Q} \quad (11)$$

$$\mathbf{g}^{K} = \mathbf{f}^{K}\cdot d_{12} \quad (12)$$

where d_{12} is the distance from the center of the molecule to the point of molecule 1 intersecting μ_{12}.

$$\mathbf{g}^{\mu\mu} = \frac{\mu^2}{r^3}\cdot(\mathbf{e}_2 + 3\cdot c_2(\mathbf{r}/r)) \quad (13)$$

$$\mathbf{g}^{QQ} = \frac{3Q^2}{4r^6}\cdot(10c_1^2 + 30c_1\cdot c_2^2 + 40\cdot(c\nu_{12} - 5c_1^2\cdot c_2^2)\cdot c_1^2.c_2^2) - \frac{3Q^2}{4r^5}\cdot(c\nu_{12} - 5c_1^2\cdot c_2^2)\cdot\mathbf{e}_2 \quad (14)$$

$$\mathbf{g}^{\mu Q} = -\frac{3\mu Q}{2r^4}(-(1+5c_1c_2 - 2c\nu_{12}) + c_{21}\cdot 5c_2)\times\frac{\mathbf{r}}{r} + \frac{3\mu Q}{2r^4}c_{21}\cdot\mathbf{e}_2 \quad (15)$$

We now define a reduced dipole density, m, and a reduced quadrupole density, Q, using the molecular volume

$$V_m = \pi\sigma^3(1 + 3L^*/2) \quad (16)$$

as a reduction factor instead of the more usual factor σ, the molecular diameter.

$$m^2 = \frac{\mu^2}{\epsilon V_m} \quad (17)$$

$$Q^2 = \frac{Q^2}{\epsilon V_m^{5/3}} \quad (18)$$

We have previously shown[14,39] that critical properties are practically independent of the molecular elongation, $L^* = L/\sigma$, as long as these definitions are applied. Simulations were carried out in the NVT ensemble using 256 particles and a leapfrog algorithm. The integration time step was taken as $\delta t^* = \delta t/\sqrt{m\sigma^2/\epsilon} = 3.5\times10^{-3}$. 5000 integration steps were performed during the equilibration period and 105 000 during the average production. For the lowest temperatures in CS_2, simulations, we considered $\delta t^* = 1.4\times10^{-2}$.

Thermodynamic states where simulations were carried out are shown in Table 3 and correspond to the temperatures and experimental densities where experimental data are available.

TABLE 3: Thermodynamic States Where Molecular Dynamics Simulations Were Carried Out

molecule	T (K)	T^*	ρ (mol/l)	ρ^*
Cl_2	184.3	0.4415	23.97	0.4768
	238.5	0.5713	22.08	0.4392
S_2C	230.2	0.3939	17.71	0.4078
	231.8	0.3967	17.68	0.4071
	248.3	0.4249	17.37	0.4000
	273.0	0.4672	16.90	0.3892
	293.9	0.5030	16.49	0.3797
	308.8	0.5285	16.19	0.3728
N_2O	298.0	0.9307	16.81	0.2344

[a] $T^* = Tk_B/\epsilon$ and $\rho^* = \rho\sigma^3$.

Therefore, a direct comparison with experiment results is possible. Different self-correlation functions can be obtained from our simulations using the Green−Kubo equations:

$$C_{AA}(t) = \lim_{\tau\to\infty}\frac{1}{\tau}\int_0^\tau A(0)\cdot A(t)\,dt = \langle A(0)\cdot A(t)\rangle \quad (19)$$

The integration of the Green−Kubo equations, and the use of the Kihara potential and a molecular framework, easily permit the direct computation of transport coefficients.[30,31] This is different from site−site potentials where an atomic framework is primarily used. These coefficients are not the main goal of our work, but they are obtained as a byproduct. Diffusion coefficients, shear viscosities, and thermal conductivities are shown in Table 4. For chlorine, agreement of our simulations with the experiment[54,55] is very good for viscosity. Agreement for S_2C is also very good for thermal conductivity, but the experiments lie slightly outside of the error bars of simulations for viscosity. Viscosity is systematically overestimated for S_2C, suggesting that our model potential is too attractive. The diffusion coefficient was obtained by the integration of the perpendicular component correlation of linear velocity because we have recently found[38] that this method reduces the integration error due to the long time tails. We find that the calculated diffusion coefficient for S_2C is too low (see Table 6), pointing out again that our model is too attractive to faithfully represent this molecule.

Closer to our main goal are the linear velocity correlation function (LVCF), the angular velocity correlation function (AVCF), and their relative Legendre polynomial correlation functions, usually called reorientation correlation functions (RCF), defined respectively as

$$C_v(t) = \langle\mathbf{v}(t)\cdot\mathbf{v}(0)\rangle \quad (20)$$

$$C_\omega(t) = \langle\boldsymbol{\omega}(t)\cdot\boldsymbol{\omega}(0)\rangle \quad (21)$$

$$C_l(t) = \langle P_l(\mathbf{e}(t)\cdot\mathbf{e}(0))\rangle \quad (22)$$

Normalized AVCF[15] for the three molecules are shown in Figure 3, showing a clear libration movement for all the molecules at low reduced temperatures. However, tracks of this movement disappear when temperature increases, even for the more elongated molecules. Relaxation times, characterizing the decay of these functions, may be defined in several ways. We use here integral correlation times defined as

$$\tau = \int_0^\infty C(t)\,dt \quad (23)$$

Reorientation correlation times of order l (LRCT) obtained in this way are denoted as τ_{il}. Asymptotic correlation times characterize the long-time exponential behavior, but they are

TABLE 4: Diffusion Coefficients, Shear Viscosity, and Thermal Conductivity for Our Models As Obtained from Molecular Dynamics Simulations[a]

molecule	T (K)	$10^9 D$ ($m^2\ s^{-1}$)	$10^4\eta$ (kg $m^{-1}\ s^{-1}$)	$10^4\eta_{exp}$ (kg $m^{-1}\ s^{-1}$)	10λ (J $K^{-1}\ m^{-1}\ s^{-1}$)	$10\lambda_{exp}$ (J $K^{-1}\ m^{-1}\ s^{-1}$)
$^{35}Cl-^{35}Cl$	184.3	0.8 ± 0.2	7.9 ± 2.0	8.3	1.6 ± 0.3	
	238.5	2.2 ± 0.3	4.5 ± 2.1	4.9	1.4 ± 0.2	
$^{35}Cl-^{37}Cl$	184.3	0.8 ± 0.2	8.1 ± 2.1		1.6 ± 0.3	
	238.5	2.1 ± 0.3	4.5 ± 2.1		1.4 ± 0.2	
$^{37}Cl-^{37}Cl$	184.3	0.8 ± 0.2	8.2 ± 2.1		1.6 ± 0.3	
	238.5	2.1 ± 0.3	4.6 ± 2.2		1.4 ± 0.2	
S_2C	230.2	0.5 ± 0.4	16.1 ± 3.1	7.5	2.0 ± 0.3	
	231.8	0.6 ± 0.2	14.2 ± 2.4	7.4	1.7 ± 0.1	
	248.3	0.8 ± 0.4	12.0 ± 1.7	6.0	1.8 ± 0.3	
	273.0	1.2 ± 0.2	7.9 ± 2.1	4.4	1.6 ± 0.1	
	293.9	1.6 ± 0.2	5.4 ± 0.6	3.6	1.6 ± 0.2	
	308.8	1.9 ± 0.2	5.3 ± 1.9	3.3	1.6 ± 0.1	1.5
N_2O	298.0	16.6 ± 0.5	0.7 ± 0.1		0.6 ± 0.1	

[a] Experimental data comes from interpolation in ref 55.

TABLE 5: Reorientation Correlation Times for the Different Molecules Considered Here

molecule	T (K)	τ_{i1} (ps)	τ_{e1} (ps)	τ_{i2} (ps)	τ_{e2} (ps)
$^{35}Cl-^{35}Cl$	184.3	2.6	2.5	1.0	0.8
	238.5	1.4	1.4	0.6	0.5
$^{35}Cl-^{37}Cl$	184.3	2.6	2.6	1.1	0.8
	238.5	1.4	1.4	0.6	0.5
$^{37}Cl-^{37}Cl$	184.3	2.7	2.6	1.1	0.8
	238.5	1.4	1.4	0.6	0.5
S_2C	230.2	8.7	8.6	2.9	2.6
	231.8	8.5	8.4	2.8	2.6
	248.3	6.4	6.4	2.2	2.0
	273.0	4.7	4.8	1.7	1.5
	293.9	3.8	3.8	1.4	1.2
	308.8	3.3	3.2	1.2	1.1
N_2O	298.0	0.5	0.6	0.3	0.3

TABLE 6: Reorientation Correlation Times of Carbon Disulfide[a]

	expt (293 K)	MT (294 K)	BMA (293 K)	ZLR (298 K)	this work (293.9 K)
$D \times 10^9$ ($m^2\ s^{-1}$)	4.2	3.85	2.6	4.21	1.6
$\tau_{i\omega} \times 10^2$ (ps)	10.3	8.8		9.9	9.9
τ_{i1} (ps)		4.0			3.8
τ_{i2} (ps)	1.3	1.4	2.1	1.3	1.4

[a] Comparison of our results with experiment[56−58] and with results coming from other models.[59−62]

usually affected by the range in which exponential behavior is considered. Therefore, we approach these times in a unique way, expressed as

$$C(\tau) = \frac{1}{e} \tag{24}$$

and denote them as τ_{el}.

These correlation times can be used to estimate the bandwidth of different kinds of spectra. Nevertheless, the comparison with the experiment must be made carefully, because usually the molecular radiation emitted interacts with the incident radiation and the band is experimentally obtained as a convolution between both the radiations

$$i(t) = \int_0^t I(t-u)E(u)\,du \tag{25}$$

where $i(t)$ is the observed time decay profile, $E(u)$ is the excitation pulse (corresponding to a δ function), and $I(t)$ is the profile which would be observed if the excitation pulse were infinitely sharp. Indeed, the band shape depends on the particular kind of pulse of the incident radiation used. However, if a short-pulse radiation, typically a laser, is used, correlation times and band broadening are related in a very simple way:

$$\Delta\omega_{il} = \frac{1}{2\pi\tau_{il}} \tag{26}$$

Reorientation correlation times for the different molecules considered here are shown in Table 5. In the case of carbon disulfide, a comparison of our results with the experiment[56−58] and with results coming from other models[59−62] is shown in Table 6. Our model gives very good results in this instance, comparing favorably with more sophisticated models.

In addition, it is easy to check that our results follow the Stokes−Einstein−Debye equation, and a plot of reorientation correlation time, τ, versus η/T shows a linear relation as shown in Figure 4. The interception of these lines with the y-axis gives the inertial term τ^0, which is related to the width of the spectrum of a classical free rotor.[63,64]

$$\tau = \frac{\eta}{T}\kappa + \tau^0 \tag{27}$$

IV. Spectroscopic Applications

The different correlation times obtained in the preceding section are related to the bandwidth by eq 26. So, τ_{e2} is related to the Raman width,[65,66] τ_{i1} to the infrared spectrum width[67] and τ_{i2} to the NMR relaxation time.[66]

The frequency shift in the liquid state can be straightforwardly obtained,[68] but we have used here a more simple treatment based on a Taylor expansion of the intermolecular potential. A similar expansion was previously used in a thermodynamic perturbation theory of monatomic liquids with excellent results.[69] The expansion of the Kihara potential around the potential minimum gives

$$U(s) \cong -\epsilon + \frac{36\epsilon(s-s_0)^2}{s_0^2} - \frac{252\epsilon(s-s_0)^3}{s_0^3} + \frac{1113(s-s_0)^4}{s_0^4} \tag{28}$$

where $s_0 = 2^{1/6}\sigma$. Truncating this expansion after the second term and retaining only the harmonic term, a corresponding force constant $k_i = 72\epsilon/s_0^2$ is obtained. Nonpolar molecules tend to align parallelly, with their center line perpendicular to the molecular axes. In this case, intramolecular and intermolecular vibrations are also perpendicular and they do not couple. However, when a quadrupole is present, a pair-favored mutual

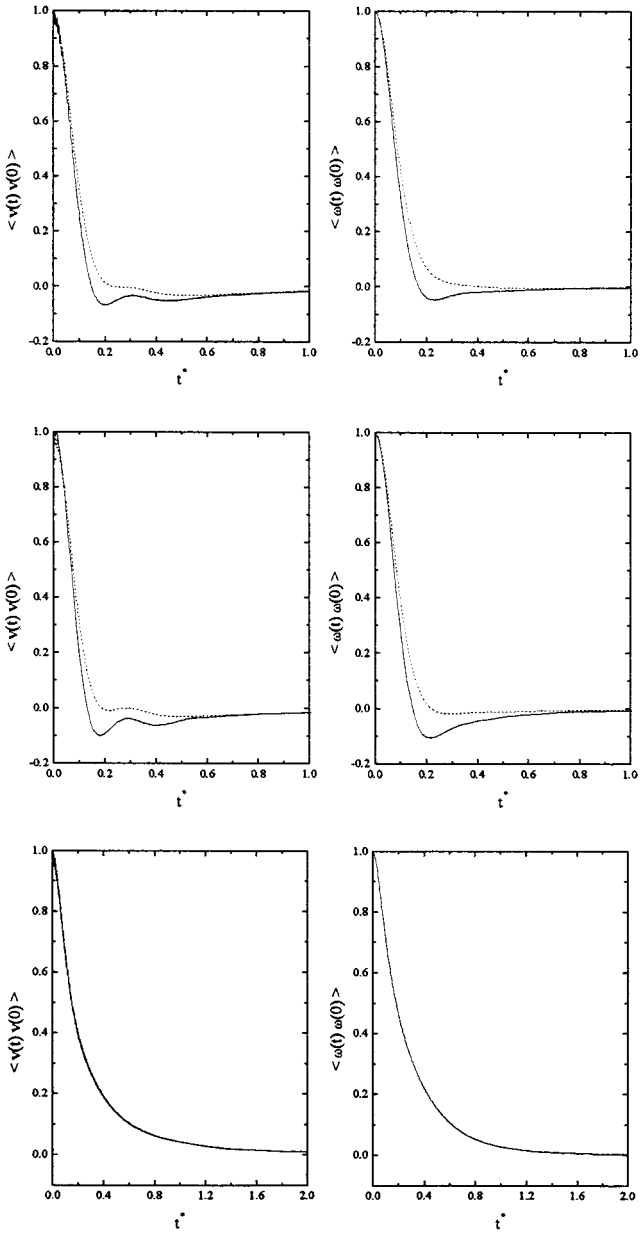

Figure 3. Angular velocity correlation functions (AVCF): (a, top) chlorine at 184.3 K (continuous line) and 238.5 K (dashed line); (b, middle) carbon disulfide at 231.8 K (continuous line) and 308.8 K (dashed line); (c, bottom) nitrous oxide at 298 K.

position is also parallel, but their centers are shifted by a quantity $L/2$. In this case, for a pair of molecules, a harmonic additional force should be added along the molecular axis. The corresponding force constant is

$$k_e = \frac{36\epsilon}{s_0^2}\left(\frac{\frac{L}{2}}{\left(s_0^2 + \frac{L^2}{4}\right)^{1/2}}\right) \tag{29}$$

and frequency shift in cm^{-1} is given by

$$\Delta\nu = \frac{1}{2\pi c}\left(\frac{k_e}{\mu}\right)^{1/2} \tag{30}$$

In our case, for the chlorine with the parameters given in Table 1, the shift frequency is estimated as $\Delta\nu_p = 0.91\ cm^{-1}$ for a

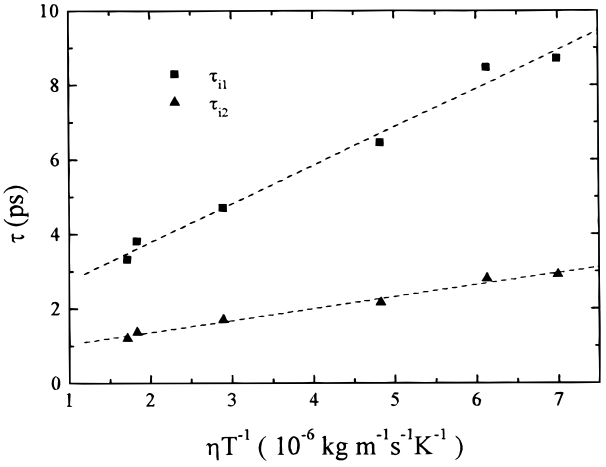

Figure 4. Reorientation correlation times (τ) versus viscosity divided by temperature (η/T) for liquid carbon disulfide.

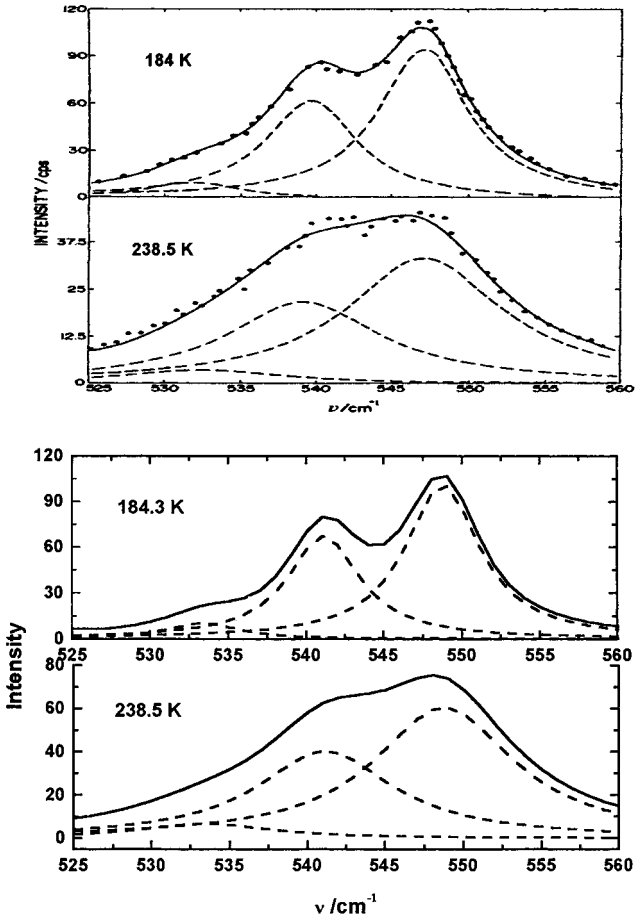

Figure 5. (a, top) Experimental Raman spectra from Topalian et al.[70] for a natural mixture of chlorine at two different temperatures. Circles are experimental points, and the line is a guide for the eye given in this reference. (b, bottom) Results obtained in this work. The Fourier transform of second-order RCF has been fitted to a Lorentzian curve.

pair of molecules. The integration to the first minimum of PCF as obtained from simulations gives z, the coordination number, and $\Delta\nu \cong z\Delta\nu_p$. Furthermore, at high densities where the liquid is far from the critical point as is our case, we can take $z \cong 12$, the largest coordination number in linear molecules. Thus, the frequency shift for chlorine is estimated as $\Delta\nu \cong 10.9\ cm^{-1}$ in very good agreement with experimental results. Figure 5a shows the experimental results from Topalian et al.[70] for a natural mixture of chlorine at two different temperatures, and Figure

TABLE 7: Bandwidths for the Isotopic Species of Molecular Chlorine[a]

$\Delta\omega$ (cm^{-1})	^{35}Cl−^{35}Cl	^{35}Cl−^{37}Cl	^{37}Cl−^{37}Cl
	$T = 184.3$ K		
$\Delta\omega_{e2}$	6.6	6.6	6.5
$\Delta\omega_{L2}$	5.7	5.6	5.6
$\Delta\omega_{G2}$	6.7	6.6	6.5
$\Delta\omega_{Raman}$[71]	7.3	7.7	6.5
	$T = 238.5$ K		
$\Delta\omega_{e2}$	10.4	10.2	10.0
$\Delta\omega_{L2}$	10.8	10.7	10.5
$\Delta\omega_{G2}$	12.2	12.0	11.9
$\Delta\omega_{Raman}$[71]	12.7	12.5	10.6

[a] Subscript L refers to a Lorentzian fit of the spectrum band and subscript G to a Gaussian fit.

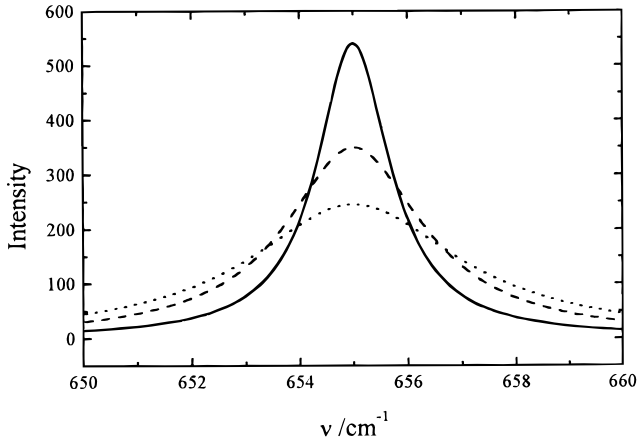

Figure 6. Symmetric stretching band for carbon disulfide at 230.2 K (continuous line), 273 K (dashed line), and 308.8 K (dotted line).

TABLE 8: Bandwidths for Carbon Disulfide[a]

$\Delta\omega$ (cm^{-1})	230.2 K	231.8 K	248.3 K	273 K	293.9 K	308.8 K
$\Delta\omega_{i1}$	0.6	0.6	0.8	1.1	1.4	1.6
$\Delta\omega_{e1}$	0.6	0.6	0.8	1.1	1.4	1.6
$\Delta\omega_{L1}$	0.6	0.6	0.8	1.1	1.3	1.6
$\Delta\omega_{G1}$	0.6	0.6	0.9	1.1	1.3	1.6
$\Delta\omega_{i2}$	1.8	1.9	2.5	3.1	3.9	4.5
$\Delta\omega_{e2}$	2.0	2.1	2.7	3.5	4.3	4.9
$\Delta\omega_{L2}$	1.6	1.7	2.2	3.1	4.0	4.7
$\Delta\omega_{G2}$	1.8	1.8	2.5	3.4	4.4	5.2
$\Delta\omega_{i2}$[57,60]	2.1[b]		2.7	4.0	4.1	6.1
$\Delta\omega_{e2}$[57,60]		2.0	2.4		3.6	4.7

[a] Subscripts as in Table 7. [b]Value at 221 K.

5b shows our results where the Fourier transform of second order-RCF has been fitted to a Lorentzian curve, subscript L in Table 7. Although the experimental curve coming from a relatively old work, and our own inherent error from the numerical Fourier transforms, make a direct comparison difficult, we think that the resemblance between the two curves is striking. Furthermore, we show in Table 7 that the corresponding bandwidths for any isotopic species of molecular chlorine show very good agreement with the experiment in all cases.

A similar study was undertaken for carbon disulfide, and the calculated shape of the symmetric stretching band at several temperatures is shown in Figure 6. Table 8 shows that the agreement between previously reported[57,60] bandwidths and those calculated in this paper remains very good. Alternative methods,[71] based on the second distribution moment of the RCF also obtainable from simulations,[30] may also be used confidently, but the band shape obtained is not very different.

V. Final Remarks

The Kihara potential has proved to be a useful tool in understanding spectral properties of linear molecular liquids. We have also shown that a large variety of molecular properties, thermodynamic and transport, as well as spectroscopic, can be obtained using a simple potential for linear molecules, notably for chlorine. Thus, the Kihara potential is used to account for the molecular shape and a point quadrupole as a simple approach to the molecular distribution charge. Clearly, in order to obtain simultaneously good results for a set of different properties, it is necessary that the intermolecular potential represent the actual intermolecular interaction very accurately. It seems that this is the case for chlorine and, to a lesser extent, for carbon disulfide. In this case, it seems that a more repulsive potential may improve the results, and we are presently considering Kihara potentials with a different repulsive exponent value. The situation is less clear for nitrous oxide, due to the scarce experimental results. We think that overall these results are quite stimulating, and we are currently exploring some other applications of these simple ideas to other spectroscopic-related problems.

Acknowledgment. This work was supported by Project PB98-0326 of Spanish DGES. S.C. and S.J. thank the Autonomous Community of Madrid and Universidad Complutense, respectively, for grants to prepare their Ph.D.'s. We also thank Brian Crilly and Linda Hamalainen for linguistic assistance.

References and Notes

(1) Hansen, J. P.; McDonald, I. R. *Theory of Simple Liquids*; Academic Press: New York, 1986.
(2) Gray, C. G.; Gubbins, K. E. *Theory of Molecular Liquids*; Clarendon: Oxford, UK, 1984; Vol. 1.
(3) Bertagnolli, H.; Schultz, E.; Chieux, P. *Ber. Bunsen-Ges. Phys. Chem.* **1989**, *93*, 88,
(4) Hall, C. D.; Johnson, K. A.; Burgess, A. N.; Winterton, N.; Howells, W. S. *Mol. Phys.* **1992**, *76*, 1061.
(5) Gay, J. G.; Berne, B. J. *J. Chem. Phys.* **1981**, *74*, 3316.
(6) De Miguel, E.; Rull, L. F.; Chalam, M. K.; Gubbins, K. E. *Mol. Phys.* **1981**, *71*, 1223.
(7) Kihara, T.; Koide, A. *Adv. Chem. Phys*. **1975**, *33*, 51.
(8) Boublík, T. *Mol. Phys.* **1976**, *32*, 1737.
(9) Lago, S.; Boublík, T. *Collect. Czech. Chem. Commun*. **1980**, *45*, 3051.
(10) Kantor, R.; Boublík, T. *Ber. Bunsen-Ges.Phys. Chem*. **1988**, *92*, 1123.
(11) Song, Y.; Mason, E. A. *Phys. Rev. A* **1990**, *42*, 4743.
(12) Vega, C.; Lago, S. *Chem. Phys. Lett.* **1991**, *185*, 516.
(13) Tang, Y.; Lu, B. C.-Y. *J. Chem. Phys.* **1994**, *100*, 3079.
(14) Vega, C.; Lago, S.; de Miguel, E.; Rull, L. F. *J. Phys. Chem*. **1992**, *96*, 7431.
(15) Lago, S.; Garzón, B.; Calero, S.; Vega, C. *J. Phys. Chem.* **1997**, *101*, 6763.
(16) Sevilla, P.; Lago, S.; Vega, C.; Padilla, P. *Phys. Chem. Liq.* **1991**, *23*, 1.
(17) Padilla, P., Lago, S.; Vega, C. *Mol. Phys.* **1991**, *74*, 161.
(18) Vega, C., Lago, S.; Padilla, P. *J. Phys. Chem.* **1992**, *96*, 1900.
(19) Pavlicek, J.; Boublík, T. *J. Phys. Chem.* **1992**, *96*, 2298.
(20) Lago, S.; López-Martín, J. L.; Garzón, B.; Vega, C. *J. Phys. Chem.* **1994**, *98*, 5355.
(21) Tang, Y.; Lu, B. C.-Y. *Mol. Phys.* **1997**, *90*, 215.
(22) Vega, C.; Frenkel, D. *Mol. Phys.* **1989**, *67*, 633.
(23) Vega, C.; Gubbins, K. E. *Mol. Phys.* **1992**, *72*, 881.
(24) Garzón, B., Lago, S.; Vega, C. *Mol. Phys.* **1999**, *96*, 123.
(25) Lundgaard, L.; Mollerup, J. M. *Fluid Phase Equilib.* **1991**, *70*, 199.
(26) Lundgaard, L.; Mollerup, J. M. *Fluid Phase Equilib.* **1992**, *76*, 141.
(27) Avlonitis, D. *Chem. Eng. Sci*. **1994**, *49*, 1173, 3193.
(28) Mehta, A. P.; Sloan, E. D. *AIChE J*. **1994**, *40*, 312.
(29) Mehta, A. P.; Dendy Sloan, E. *AIChE J*. **1996**, *42*, 2036.
(30) MacDowell, L. G.; Garzón, B.; Calero, S.; Lago, S. *J. Chem. Phys.* **1997**, *106*, 4753.
(31) Calero, S.; Garzón, B.; MacDowell, L. G.; Lago, S. *J. Chem. Phys.* **1997**, *107*, 2034.
(32) Williamson, D. C.; Guevara, Y. *J. Phys. Chem.* **1999**, *103*, 7522.

(33) Del Río, F.; Ramos, J. E.; McLure, I. *J. Phys. Chem.* **1998**, *102*, 10568.
(34) Ramos, J. E.; del Río, F.; McLure, I. *J. Phys. Chem.* **1998**, *102*, 10576.
(35) Erman, B.; Bahar, I.; Jernigan, R. L. *J. Chem. Phys.* **1997**, *107*, 2046.
(36) Kuchta, B.; Etters, R. D.; Le Sar, R. *J. Chem. Phys.* **1992**, *97*, 5662.
(37) Steele, D., Yarwood, J., Eds. *Spectroscopy and Relaxation of Molecular Liquids*; Elsevier: Amsterdam, 1991.
(38) Calero, S.; Lago, S.; Garzón, B. *J. Chem. Phys.* **1999**, *111*, 5434.
(39) Garzón, B.; Lago, S.; Vega, C.; Rull, L. F. *J. Chem. Phys.* **1995**, *102*, 7204.
(40) Wormald, C. J.; Eyers, J. M. *J. Chem. Soc., Faraday Trans. 1* **1988**, *84*, 3097.
(41) Graham, C.; Imrie, D. A.; Raab, R. E. *Mol. Phys.* **1998**, *93*, 1, 49.
(42) Battaglia, M. R.; Buckingham, A. D.; Neumark, D.; Pierens, R. K.; Williams, J. H. *Mol. Phys.* **1981**, *43*, 1015.
(43) Armstrong, B. *J. Chem. Eng. Data* **1981**, *26*, 168.
(44) Simmrock, K. H.; Janowsky, R.; Ohnsorge, A. *Critical Data of Pure Substances*; Chemistry Data Series II; DECHEMA: Frankfurt, 1986; Vol. I.
(45) Reid, R. C.; Prausnitz, J. M.; Poling, B. E. *The Properties of Gases and Liquids*, 4th. ed.; McGraw-Hill: Singapore, 1988.
(46) Moore, W. J. *Physical Chemistry*, 5th ed.; Longman: London, 1972.
(47) Padilla, P.; Lago, S. *Fluid Phase Equilib.* **1989**, *48*, 53.
(48) Petersson, G. A.; Al-Laham, M. A. *J. Chem. Phys.* **1991**, *94*, 6081.
(49) Petersson, G. A.; Bennett, A.; Tensfeldt, T. G.; Al-Laham, M. A.; Shirley, W. A.; Mantzaris, J. *J. Chem. Phys.* **1988**, *89*, 2193.
(50) Clark, T.; Chandrasekhar, J.; Spitznagel, G. W.; Schleyer, P. V. R. *J. Comput. Chem.* **1983**, *4*, 294.
(51) Frisch, M. J.; Pople, J. A.; Binkley, J. S. *J. Chem. Phys.* **1984**, *80*, 3265.
(52) Kristof, T.; Liszi, J.; Szalai, I. *Mol. Phys.* **1996**, *89*, 931.
(53) Kristof, T.; Liszi, J.; Szalai, I. *Mol. Phys.* **1997**, *90*, 1031.
(54) *Handbook of Chemistry and Physics*, 80th ed.; CRC Press: Boca Raton, FL, 1999.
(55) Lide, D. R.; Kehiaian, H. V. *CRC Handbook of Thermophysical and Thermochemical Data*; CRC Press: Boca Raton, FL, 1994.
(56) Woolf, L. A. *J. Chem. Soc., Faraday Trans. 1* **1982**, *78*, 583.
(57) Cox, T. I.; Battaglia, M. R.; Madden, P. A. *Mol. Phys.* **1979**, *38*, 1538.
(58) Spiess, H. W.; Schweitzer, D.; Haeberlein, U.; Hauser, K. H. *J. Magn. Reson.* **1971**, *5*, 101.
(59) Tildesley, D. J.; Madden, P. A. *Mol. Phys.* **1981**, *42*, 1137.
(60) Tildesley, D. J.; Madden, P. A. *Mol. Phys.* **1983**, *48*, 129.
(61) Böhm, H. J.; Meissner, C.; Ahlrichs, R. *Mol. Phys.* **1984**, *53*, 651.
(62) Zhu, S. B.; Lee, J.; Robinson, G. W. *Mol. Phys.* **1988**, *65*, 65.
(63) Kivelson, D. *Discuss. Faraday Soc*. **1977**, *11*, 7.
(64) Alms, G. R.; Bauer, D. R.; Brauman, J. I.; Pecora, R. *J. Chem. Phys.* **1973**, *59*, 5310.
(65) Bartoli, F. J.; Litovitz, T. A. *J. Chem. Phys.* **1972**, *56*, 413.
(66) Zhu, B.; Lee, J.; Robinson, G. W. *Mol. Phys.* **1988**, *65*, 65.
(67) Rothschild, W. G. *J. Chem. Phys.* **1972**, *57*, 991.
(68) Le Sar, R. *J. Chem. Phys* **1987**, *86*, 4138.
(69) Lago, S. *J. Chem. Phys.* **1985**, *83*, 2405.
(70) Topalian, H.; Maguire, J. F.; McTague, J. P. *J. Chem. Phys.* **1979**, *71*, 1884.
(71) Kirillov, S. A. *Chem. Phys. Lett*. **1999**, *303*, 37.